International Journal of Control Science and Engineering 2016, 6(2): 23-37
DOI: 10.5923/j.control.20160602.01

Control of Periodic and Chaotic Motions in a Cantilever Beam with Varying Orientation under Principal Parametric Resonance

Usama H. Hegazy

Department of Mathematics, Faculty of Science, Al-Azhar University, Gaza, Palestine

Abstract The principal parametric nonlinear response and control of a cantilever beam with varying orientation under direct and parametric excitations are analyzed and studied. The cantilever beam is modeled by a second order nonlinear ordinary differential equation. Various control techniques are proposed and numerical integration is performed to investigate the effectiveness of the applied controllers and time histories of the beam at the principal parametric resonance case. Approximate solution is sought applying the method of the multiple scales and the effect of the parameters on the stability of the nonlinear response is examined.

Keywords Control, Periodic motion, Chaotic motion, Principal parametric resonance

1. Introduction

The stability and bifurcation of subharmonic motions of a parametrically excited flexible rod are investigated using Melnikov asymptotic method [1]. The vibration control of one dimensional cantilever beam of varying orientation under external and parametric excitations is studied and analyzed. The cubic velocity feedback control is applied and the method of multiple scaled is utilized to construct the modulation equations of the amplitudes and phases. Numerical simulations are performed to investigate the effects of system parameters and the stability [2]. The nonlinear vibration and saturation phenomenon are analyzed in the controlled hinged-hinged flexible beam. The performance of different control techniques are studied and found that the oscillations of the system can be controlled actively via negative velocity feedback. Effects of system parameters are also investigated [3]. A control law based on quintic velocity feedback is proposed to reduce the vibrations of one dimensional cantilever beam under primary and parametric excitations. Numerical simulations are performed to verify analytical results obtained using the multiple scales method and to detect chaos and unbounded motions [4]. The chaotic motion of the nonlinear cantilever beam under harmonic axial excitation and transverse excitations at the free end is investigated. A new force control approach is proposed to control the chaotic response of the system considering the case of two-to-one internal resonance, principal parametric resonance-1/2 subharmonic resonance for the in-plane mode and fundamental parametric resonance-primary resonance for the out-of-plane mode [5, 6]. Subharmonic resonances of order one-half with fundamental parametric resonances are analyzed and studied in a single-degree-of-freedom system with quadratic and cubic nonlinearities. The steady-state solutions and their stability are determined applying the method of multiple scales [7]. The nonlinear response in the first vibration mode of a clamped-clamped beam subject to a subharmonic resonance of order one-half is investigated theoretically and experimentally. The multi-mode Galerkin method is used to discretize the governing partial differential equation into a set of coupled ordinary differential equations that are solved using the multiple scales method [8]. The nonlinear response of a post-buckled beam under harmonic axial load is analytically studied with five subharmonic resonances utilizing the multiple scales method. The steady-state solutions are obtained and their stability are investigated [9]. The method of multiple scales is used to obtain analytical solution for the nonlinear differential equations describing the motion of the controlled electromechanical system with time-varying stiffness. Negative linear, quadratic, and cubic velocity feedback controllers are applied to the system and investigated. It is found that the vibration of the seismograph model is best controlled via the negative velocity feedback [10]. A nonlinear cantilever beam of varying orientation with time-delay subject to direct and parametric excitations is studied at the primary and parametric resonances. The first order approximation of the response is obtained using the multiple scales method, where the time delay is presented in

* Corresponding author:
u.hejazy@alazhar.edu.ps (Usama H. Hegazy)
Published online at http://journal.sapub.org/control

the proportional feedback and the derivative feedback [11]. The Melnikov method is used to determine the homoclinic and heteroclinic chaos in the micromechanical resonators. Numerical simulations including basin of attraction and bifurcation diagrams reveal the effect of parametric excitation on the system transition to chaos and confirm analytical predictions. Moreover, the time-varying stiffness is introduced to control the chaotic motion of the system [12]. The nonlinear response of a Timoshenko beam having a randomly varying stiffness and loss factor at its support is studied under harmonic moving load. The mean value and standard deviation of the beam responses are calculated using the first-order two dimensions perturbation method [13]. The numerical Runge-Kutta method with variable step-size is applied to explore the subharmonic dynamics of an axially accelerating beam. It is found that the variation of the mean value of the speed and the amplitude of the speed affect the periodic, quasiperiodic, and chaotic responses of the system [14]. The method of multiple scales is used to analyze the nonlinear flexural vibrations of a microcantilever beam with a piezoelectric actuator layer on the top side of the beam. The obtained analytical and numerical results are verified experimentally [15]. An acceleration feedback controller technique is proposed to reduce the oscillations in a class of multi degrees-of-freedom mechanical systems. The control cost and robustness of the controller are taken into account when choosing the control parameters. Numerical simulations are carried out to verify analytical predictions. A nonlinear velocity feedback control method for inducing natural oscillations in a class of two degrees-of-freedom mechanical systems is proposed and investigated [16, 17]. A new control method that combines sliding mode control (SMC) and positive position feedback control (PPF) is proposed to suppress the vibration of a beam subjected to a moving mass. Combining both control methods is found to overcome problems arise when applying each method separately. Numerical examples are given to demonstrate the effectiveness of the proposed method [18]. The positive position feedback (PPF) method, the integral resonant control (IRC) method and a new nonlinear integral positive position feedback (NIPPF) are considered and analyzed for vibration suppression of nonlinear systems. The method of multiple scales is utilized to solve the closed-loop system. It is found that the NIPPF controller has excellent results compared to the other two methods as it reduces the vibration at the exact resonant frequency. Also the subsequent peaks in the frequency domain are significantly suppressed [19]. The horizontal vibration of a magnetically levitated system with quadratic and cubic nonlinearities under primary and parametric excitations is investigated. A proportional-derivative controller is applied to suppress the oscillations of the resonant system. The method of multiple scales is used to obtain a second order approximate solution, which is compared numerically [20]. Displacement-velocity feedback and a linear classical control algorithm with a time varying gain matrix are proposed to reduce the vibration of a nanotube structure under a moving nanoscale particle. The performance of the applied control method with different numbers of the controlled modes and control forces along with the effects of the moving nanoparticle velocity and slenderness deflection are studied [21]. An electromechanical transducer, which consists of a mechanical oscillator linked to an electronic circuit is studied and two nonlinear control techniques are proposed to improve the transient response and to keep the system into the required periodic motion by avoiding both the chaotic and resonant behaviors. The control techniques are the optimal linear feedback and the state dependent Riccati equation. Numerical simulations are carried out to compare both methods and the energy transfer pumping between the electrical part and mechanical part is investigated [22].

In this study, controlling the periodic and chaotic nonlinear responses of a nonlinear beam with varying orientation under principal parametric resonance case are studied numerically and analytically. The multiple scales analytical method and Rung-Kutta numerical method are applied and the stability of the beam model and effect of the system parameters are investigated using the time-histories, the phase portraits and the frequency response curves at the principal parametric resonance condition.

2. Mathematical Model

The governing equation of motion to be studied and solved has the from

$$\ddot{x} + +\omega^2 x + \varepsilon(2\mu\dot{x} + \beta x^2 + \gamma x^3) = \varepsilon(2f_1 \sin(\Omega_1 t)\cos(\alpha) + 2xf_2 \sin(\Omega_2 t)\sin(\alpha)) + T \quad (1)$$

where, x ,$\dot{x}$ and $\ddot{x}$ are the displacement, velocity and acceleration, ε is a small bookkeeping perturbation parameter, μ is the damping coefficient, ω is the natural frequency, β and γ are quadratic and cubic nonlinear terms, f_1 and f_2 are the external and parametric forcing amplitudes, $\Omega_{1,2}$ are the forcing frequencies, α is the orientation angle of the beam and T is a control input.

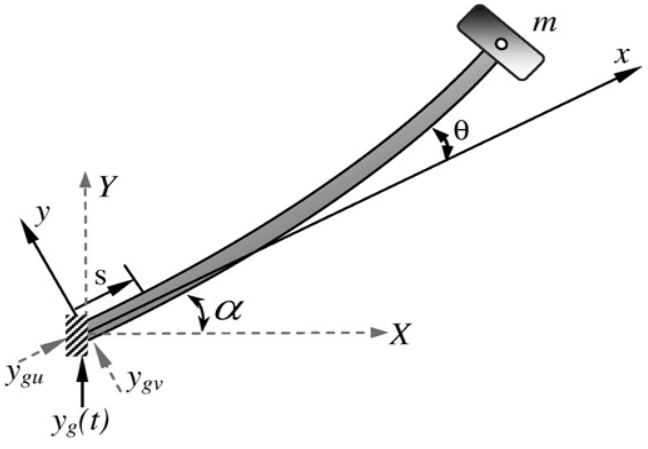

Figure 1. The considered model of a cantilever beam

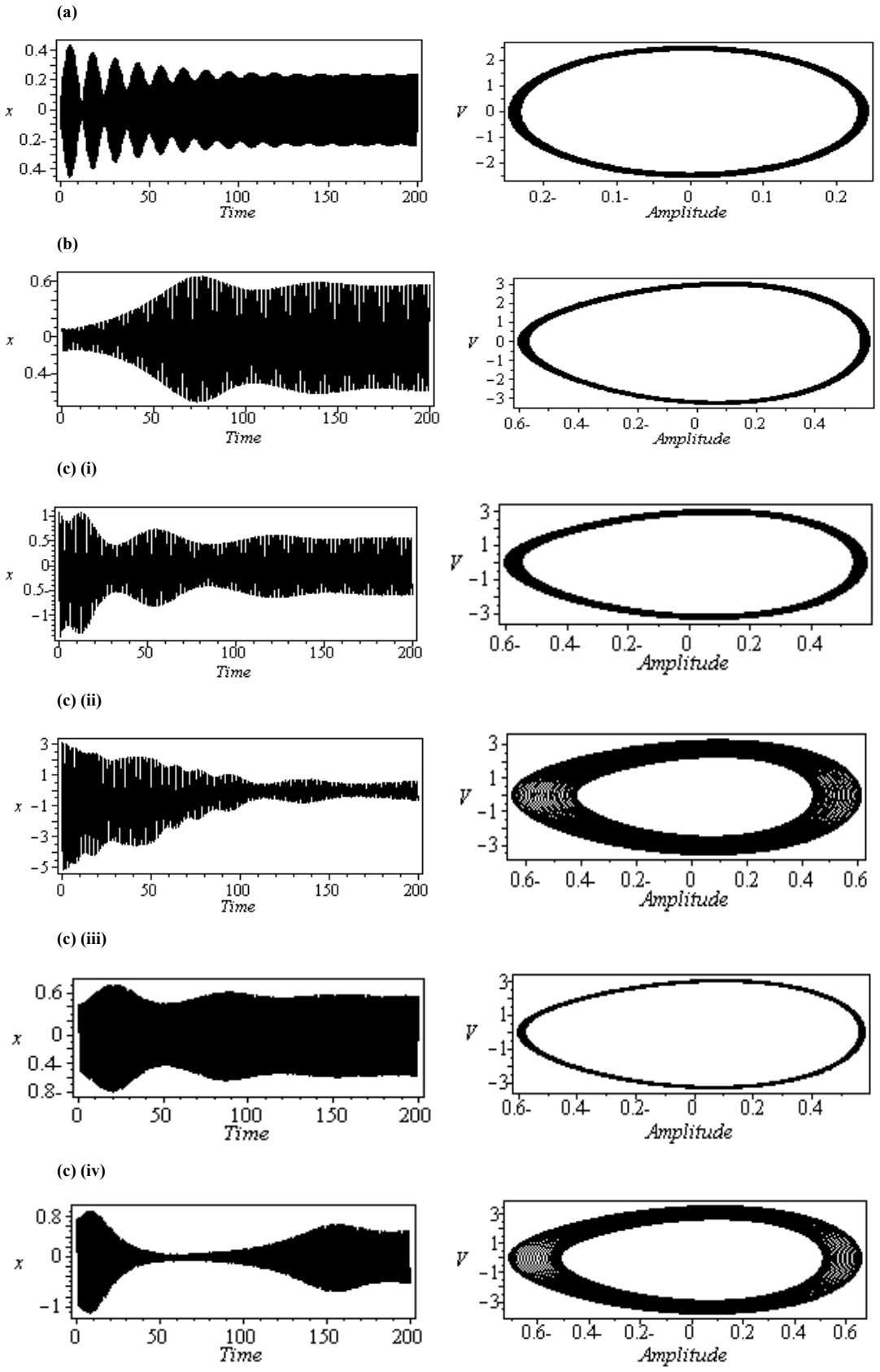

(a) Non-resonant time response, (b) Principal parametric resonant time response, (c) Effect of initial conditions on system behavior at resonance: (i) $x(0)$=1.5, (ii) $x(0)$=2.8., (iii) $\dot{x}(0) = 2.0$ and (iv) $\dot{x}(0) = 4.0$

Figure 2. Numerical solution of the cantilever beam

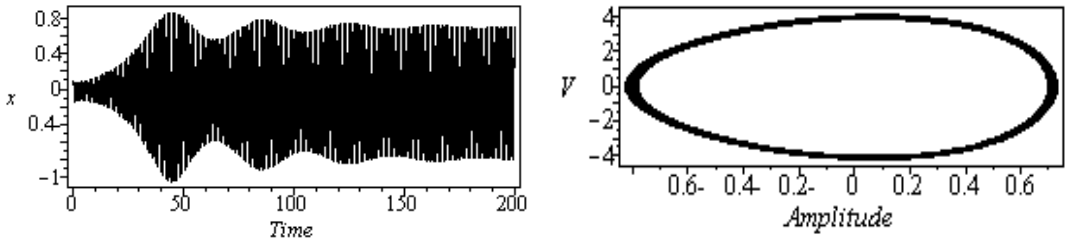

(a) α = 30°

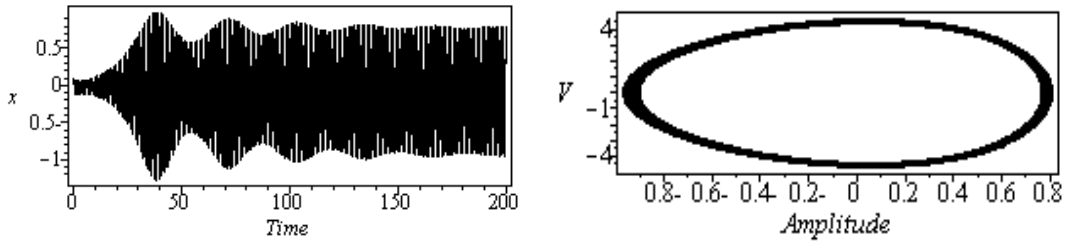

(b) α = 50°

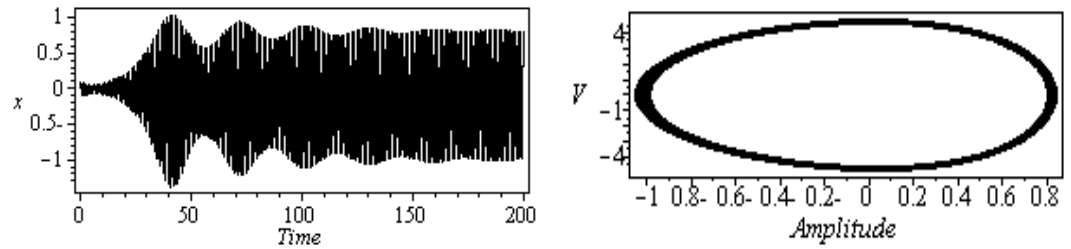

(c) α = 70°

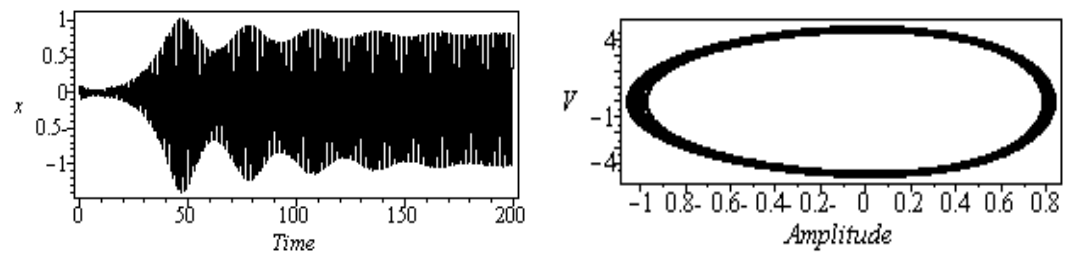

(d) α = 80°

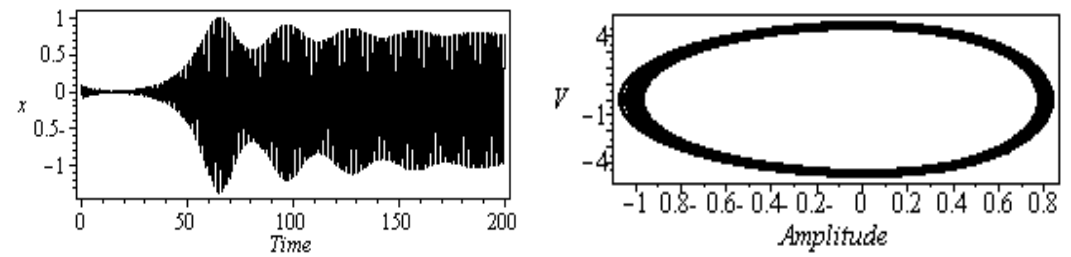

(e) α = 90°

Figure 3. Effect of the orientation angle at principal parametric resonance

3. Time-History and Phase-Portrait Solution

Equation (1) is solved numerically using Runge-Kutta fourth order and the time histories and final phase portraits are plotted when the values for the system parameters are chosen as follows:

μ=0 .02, ω = 10.9, f_1 = 1.5, f_2 = 1.2, Ω_1 = 10.4, Ω_2 = 9.9, β = 10.0, γ = 2.03, $\alpha = 10^o$ with initial condition $x(0)$=0.1 and zero initial velocity, unless otherwise specified.

Figure 2(a) shows a modulated vibration for the beam at nonresonance, while Fig. 2(b) shows the oscillations of the system at the principal parametric resonance case ($\Omega = 2\omega$) and the final phase-planes indicate fine limit cycles for both cases. Comparing the nonresonant and resonant solutions illustrates that the maximum steady-state amplitude at resonance has increased to about 115%. The principal parametric resonance solution will be considered as basic case in the following investigations. It can be seen from Figs. 2(c) (i - iv), that as the initial conditions are different, the steady-state solutions are different.

In Fig. 3, the principal parametric time response solution for four different values of the orientation angle α is shown. It is seen that as the orientation angle is increased, the motion of the beam becomes more modulated and the transient time increases. The amplitude of the response is also increased when α increases to 70°, but more increase does not significantly change the amplitude, which may lead to a saturation phenomenon occurrence.

Fig. (4) shows the effect of varying the external force f_1 on the amplitude of the model. As f_1 increases up to 100.0, Fig. 4(a), the amplitude increases. Further increase does not significantly change the amplitude which indicate a saturation phenomenon as shown in Figs. 4(b) and 4(c).

The effect of the parametric forcing amplitude f_2 is shown in Fig. 5, which represents the time-series solution (t, x) and the phase-plane (x, v) at principal parametric resonance, where v denotes the velocity. Considering Fig. 2(b) as basic case for comparison. It can be seen from Fig. 5(a) that as f_2 is increased to 50.0, a sever chaotic motion occurs with multi-limit cycles. When f_2 is increased to 100.0, Fig. 5(b), the chaotic behavior persists for the time $0 < t < 150.0$, then it becomes periodic with fine limit cycle. This transition from chaotic motion at the beginning to periodic motion till the end is also observed in Figs. 5(c)-5(e) as f_2 increases further.

3.1. Effects of Different Parameters

Figure 6 shows the effect of different coefficients on the steady-state amplitude of the resonant beam, which is summarized in table 1.

Table 1. Effects of the system parameters

System parameters	Fig. No.	amplitude
Linear damping coefficient μ	Fig. 6a	M.D*.
Natural frequency ω	Fig. 6b	**
Cubic nonlinear parameter γ	Fig. 6c	M.D*.
Quadratic nonlinear parameter β	Fig. 6d	M.D*.
External excitation amplitude f_1	Fig. 6e	M.I*.
Parametric excitation amplitude f_2	Fig. 6f	M.I*.

where
M.I. denotes that the amplitude is a monotonic increasing function in the parameter.
M.D. denotes that the amplitude is a monotonic decreasing function in the parameter.
* A saturation phenomena is noticed as the parameter is increased.
** The amplitude has two peaks as ω is varied, the maximum peak occurs at the principal parametric resonance.

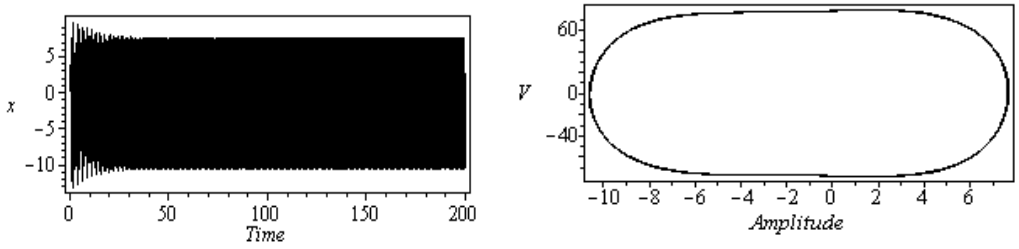

(a) $f_1 = 100.0$

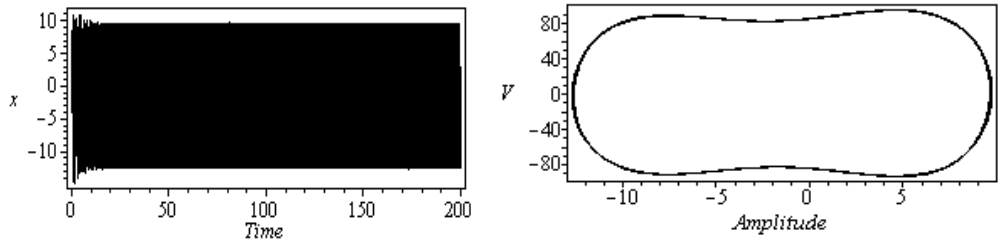

(b) $f_1 = 400.0$

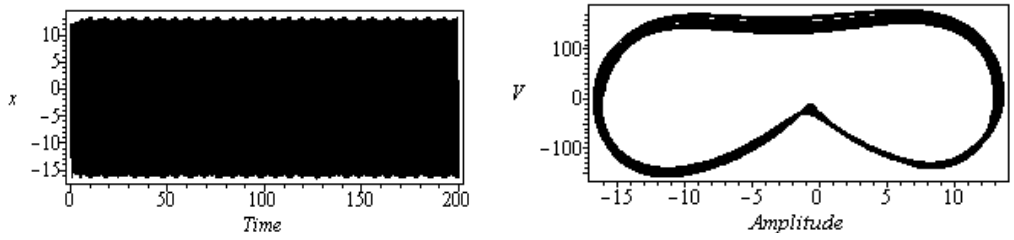

(c) $f_1 = 1000.0$

Figure 4. Effect of the external excitation at principal parametric resonance

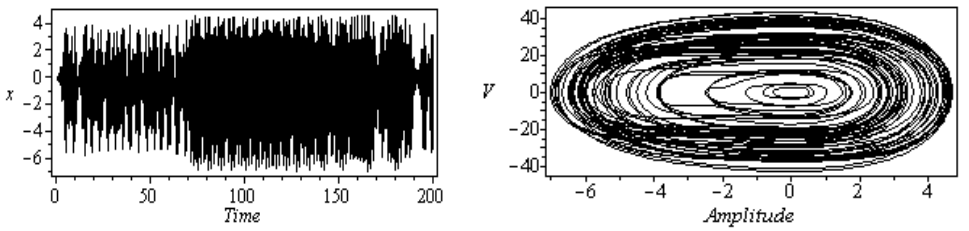

(a) $f_2 = 50.0$

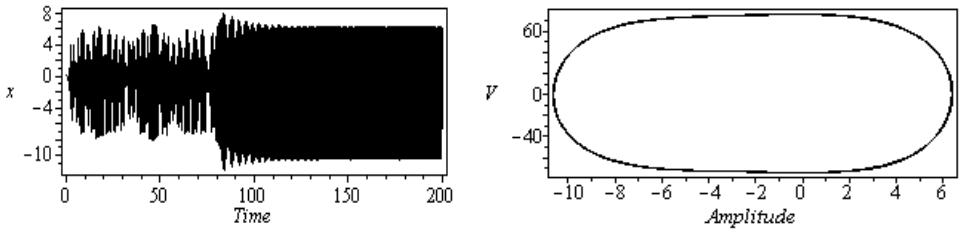

(b) $f_2 = 100.0$

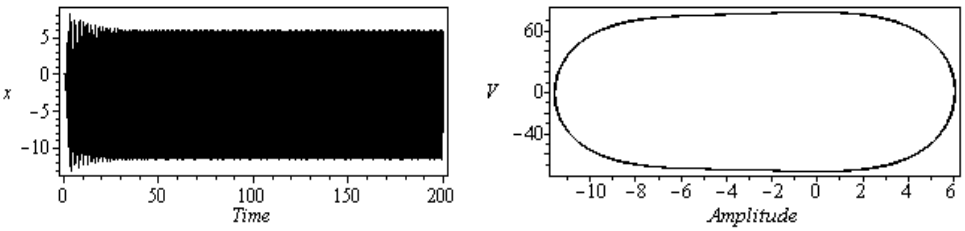

(c) $f_2 = 200.0$

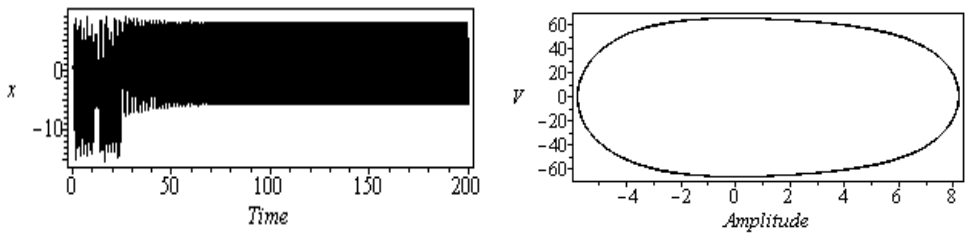

(d) $f_2 = 400.0$

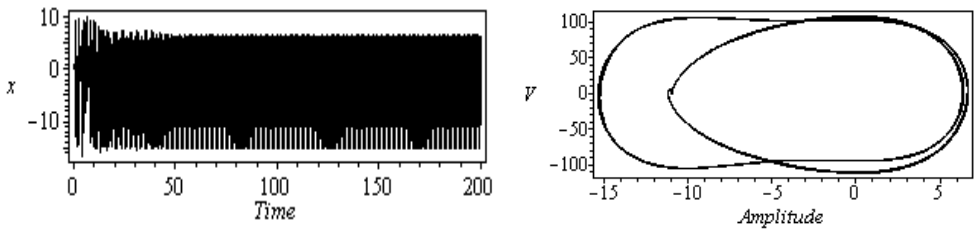

(e) $f_2 = 500.0$

Figure 5. Effect of the parametric excitation at principal parametric resonance

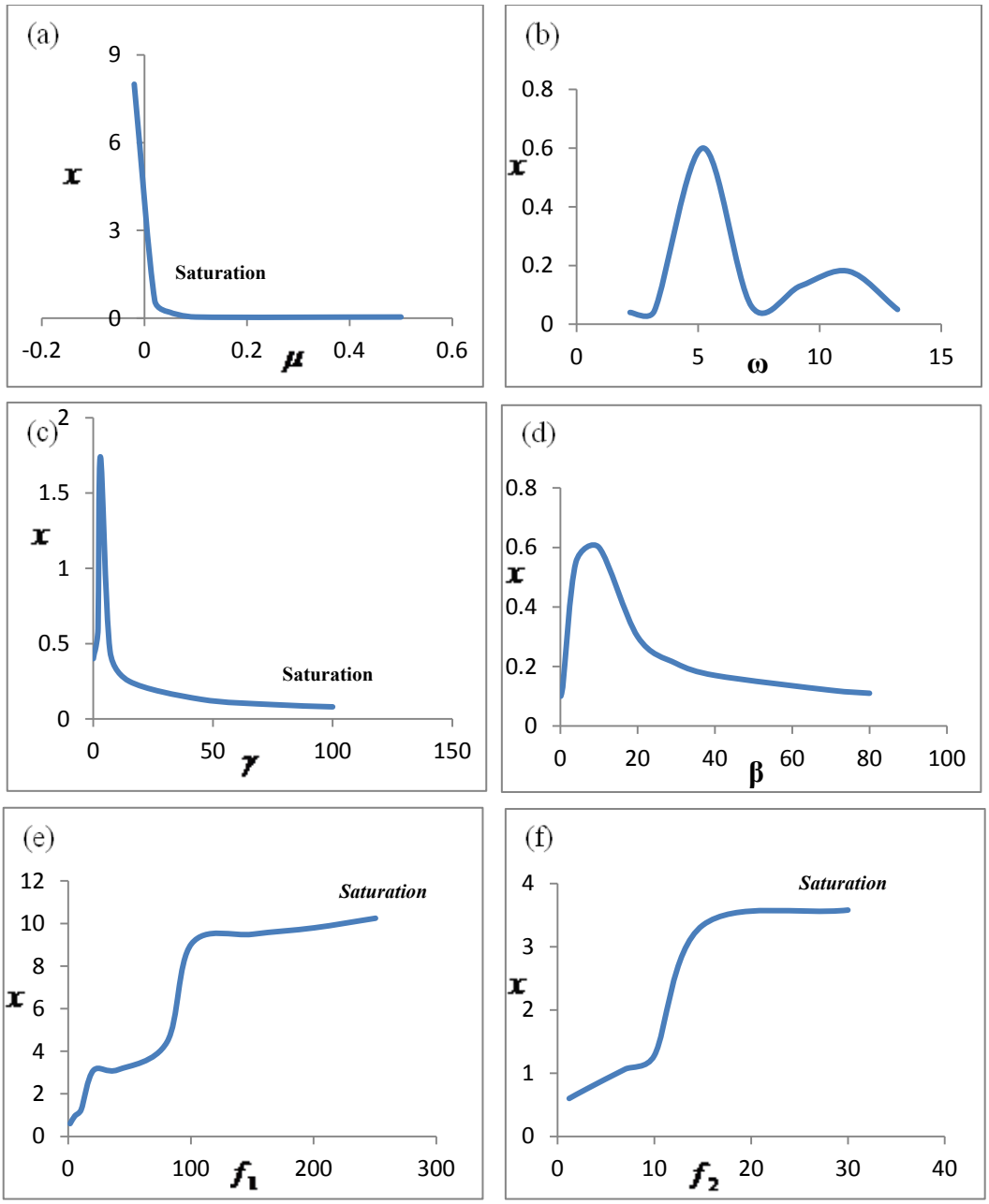

Figure 6. Effect of the parameters at principal parametric resonance - numerical integration of the system: (*x*-axis: the parameter, *y*-axis: *x*-amplitude)

3.2. Effect of the Gain Coefficient *G*

Figure 7 shows the effect of suppressing the steady-state amplitude of the beam for various values of the gain when different controllers are applied. Three position feedback (PF) laws $(T = \varepsilon G x^n, n = 1,2,3)$ and three negative velocity feedback (VF) laws $(T = -\varepsilon G \dot{x}^n, n = 1,2,3)$. The effectiveness of each control law is evaluated and represented by E_a = steady-state amplitude of the system before control / steady-state amplitude of the system after control, which is calculated at saturation beginning. Comparing the effectiveness of these controllers.

It is noticed from Fig. 7(a) that:

- $\mathbf{E_a}$ = 15.0, 15.0, and 6.0 and saturation begins at *G* greater than 5.0, 15.0, and 70.0 to control the system when applying linear (L), quadratic (Q), and cubic (C) PF controllers, respectively. This means that the LPF controller ($T = \varepsilon G x$) is the best one among PF controllers.

Whereas Fig. 7(b) indicates that:

- $\mathbf{E_a}$ = 1.2, 1.2, and 1.2 and saturation begins at *G* greater than 0.5, 0.5, and 0.2 to control the system when applying linear (L), quadratic (Q), and cubic (C) VF controllers, respectively. This means that the CVF controller ($T = -\varepsilon G \dot{x}^3$) is the best one among VF controllers.

In the next section we shall investigate the performance of the LPF and the negative CVF analytically using the method of multiple scales.

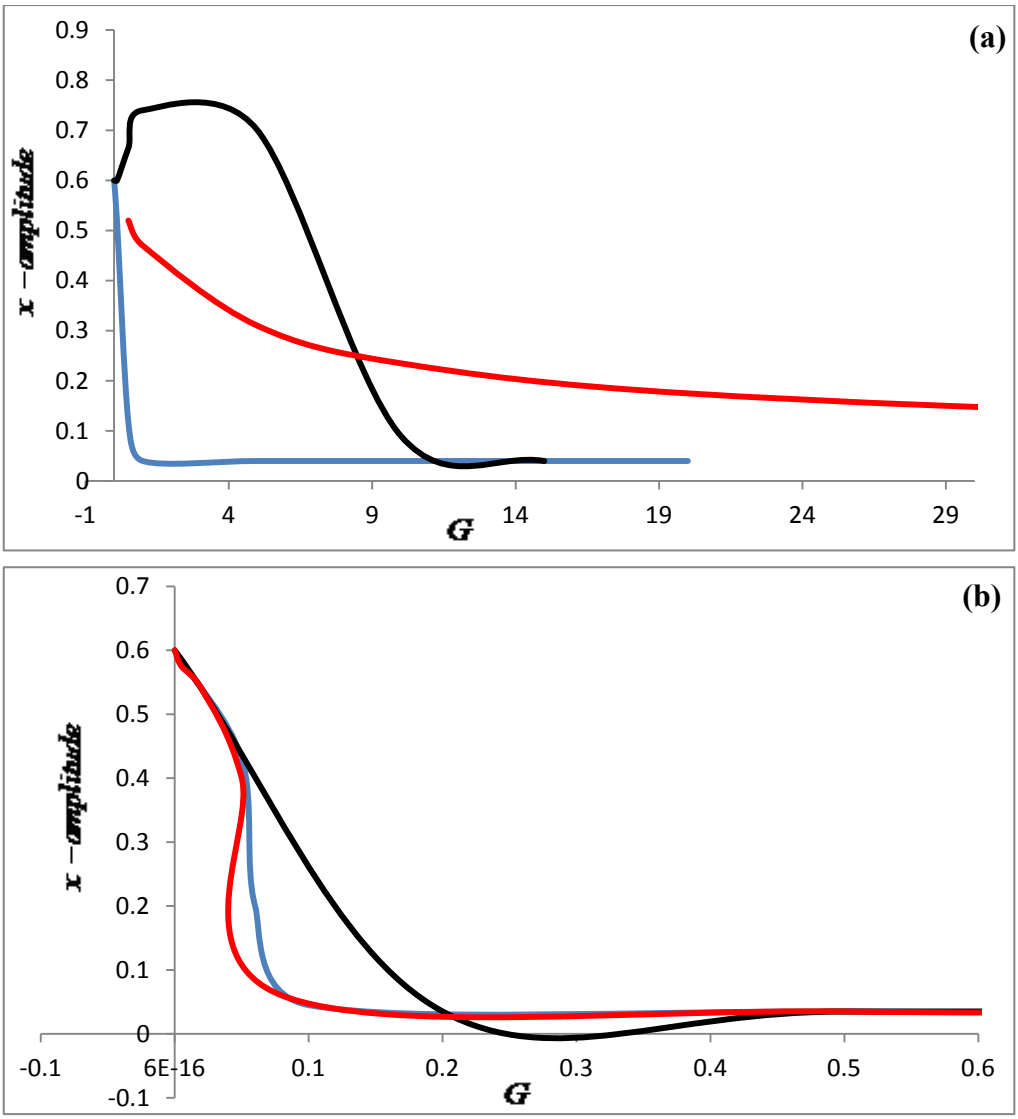

(a) LPF (blue), QPF (black) and CPF (red) controllers
(b) Negative LVF (blue), QVF (black) and CVF (red) controllers

Figure 7. Effect of the gain for various control laws at principal parametric resonance - numerical solution: (*x*-axis: the gain, *y*-axis: *x*-amplitude)

4. Analytical Solution

In this section the approximate solution of the nonlinear system, Eq. (1) with the two effective controllers is analyzed applying the method of multiple scales.

4.1. Linear Position Feedback Controller (LPF)

Setting $T = \varepsilon G x$ in Eq. (1) and assuming x is in the form

$$x(\mathrm{T}_0, \mathrm{T}_1) = x_0(\mathrm{T}_0, \mathrm{T}_1) + \varepsilon x_1(\mathrm{T}_0, \mathrm{T}_1) + \ldots\ldots\ldots \quad (2)$$

where $\mathrm{T}_0 = t$ is the fast time scale and $\mathrm{T}_1 = \varepsilon \mathrm{T}_0 = \varepsilon t$ is the slow time scale. The time derivatives are expressed as

$$\frac{d}{dt} = \mathrm{D}_0 + \varepsilon \mathrm{D}_1 + \ldots\ldots, \quad \frac{d^2}{dt^2} = \mathrm{D}_0^2 + 2\varepsilon \mathrm{D}_0\mathrm{D}_1 + \ldots\ldots,$$

$$\mathrm{D}_0 = \frac{\partial}{\partial T_0}, \quad \mathrm{D}_1 = \frac{\partial}{\partial T_1}.$$

Equating the coefficient of same powers of ε yields:

$$O(\varepsilon^0) : (\mathrm{D}_0^2 + \omega^2)x_0 = 0 \quad (3)$$

$$O(\varepsilon) : (\mathrm{D}_0^2 + \omega^2)x_1 = -2\,\mathrm{D}_0\mathrm{D}_1\,x_0 - 2\mu\,\mathrm{D}_0\,x_0 - \beta x_0^2 - \gamma x_0^3 + 2f_1 \sin(\Omega_1 t)\cos(\alpha) + 2x_0 f_2 \sin(\Omega_2 t)\sin(\alpha) + G x_0. \quad (4)$$

The general solution of Eq. (3) is given by

$$x_0 = A(T_1)e^{i\omega T_0} + \overline{A}(T_1)e^{-i\omega T_0} \quad (5)$$

Substituting Eq. (5) into Eq. (4), gives

$$(D_0^2+\omega^2)x_1=[-2i\omega A'-2i\omega\mu A-3\gamma A^2\bar{A}+GA]e^{i\omega T_0}-\beta A^2e^{2i\omega T_0}-\gamma A^3e^{3i\omega T_0}-2\beta A\bar{A}-if_1e^{i\Omega_1 T_0}\cos(\alpha)-if_2Ae^{i(\omega+\Omega_2)T_0}\sin(\alpha)+if_2Ae^{i(\omega-\Omega_2)T_0}\sin(\alpha)+cc. \quad (6)$$

The principal parametric resonance will be considered and studied. It occurs when Ω_2 is very close to twice ω, which is expressed as

$$\Omega_2-\omega=\omega+\varepsilon\sigma \quad (7)$$

From Eq. (6) the secular terms, which result in unbounded solution, are eliminated and the solvability condition yield

$$-2i\omega A'-2i\omega\mu A-3\gamma A^2\bar{A}+GA-if_2\bar{A}e^{i\sigma T_1}\cos(\alpha)=0 \quad (8)$$

Using the following polar form expression in Eq. (8)

$$A=\frac{1}{2}a(T_1)e^{i\theta(T_1)} \quad (9)$$

where a,θ are the steady-state amplitude and phase of the motion. Then Separating imaginary and real parts, and setting $v=\sigma T_1-2\theta$ we obtain

$$a'=-\mu a-\frac{f_2a}{2\omega}\cos v\cos(\alpha) \quad (10)$$

$$v'a=\sigma a-\frac{3}{8\omega}\gamma a^3+\frac{1}{2\omega}Ga+\frac{f_2a}{2\omega}\sin v\cos(\alpha) \quad (11)$$

The steady-state solutions correspond to constant a, v that is $a'=v'=0$ Thus Eqs. (11) and (12) can be reduced to the following nonlinear algebraic equations

$$\mu=-\frac{f_2}{2\omega}\cos v\cos(\alpha) \quad (12)$$

$$\sigma-\frac{3}{8\omega}\gamma a^2+\frac{1}{2\omega}G=-\frac{f_2}{2\omega}\sin v\cos(\alpha) \quad (13)$$

Then we obtain the following frequency response equation

$$\frac{9}{64\omega^2}\gamma^2a^4-(\frac{3}{4\omega}\sigma\gamma+\frac{3}{8\omega^2}G\gamma)a^2+(\frac{\sigma G}{\omega}+\frac{G^2}{4\omega^2}+\mu^2+\sigma^2)-\frac{f_2^2}{4\omega^2}\cos^2(\alpha)=0 \quad (14)$$

4.2. Negative Cubic Velocity Feedback Controller (CVF)

Setting $T=\varepsilon G\dot{x}^3$ in Eq. (1) and following the same procedure as in LPF controller, considering the principal parametric resonance case, one obtains the solvability condition as

$$-2i\omega A'-2i\omega\mu A-3\gamma A^2\bar{A}+3i\omega^3GA^2\bar{A}-if_2\bar{A}e^{i\sigma T_1}\cos(\alpha)=0$$

And the frequency response equation is given by

$$\frac{9}{64}(\frac{\gamma^2}{\omega^2}+\omega^4G^2)a^4+\frac{3}{4}(\mu\omega^2G-\frac{\sigma\gamma}{\omega})a^2+\mu^2+\sigma^2-\frac{f_2^2}{4\omega^2}\cos^2(\alpha)=0 \quad (15)$$

Next, we study the problem of stability of linear (trivial) solutions with the two controllers.

4.3. Trivial Solution

To determine the stability of the trivial solutions, one investigates the principal parametric resonant solution with LPF control by introducing the following Cartesian form

$$A_0=\frac{1}{2}\left(p_1+iq_1\right)e^{\frac{i\sigma T_1}{2}} \quad (16)$$

into the linearized form of Eq. (9), that is into

$$-2i\omega(A_0'+\mu A_0)+GA-if_2\bar{A}e^{i\sigma T_1}\cos(\alpha)=0 \quad (17)$$

where p_1, q_1 are real, then separating real and imaginary parts, gives the following eigen-value equation

$$\lambda^2+2\left(2\mu+\frac{f_2}{\omega}\cos(\alpha)\right)\lambda+\left(2\mu+\frac{f_2}{\omega}\cos(\alpha)\right)^2-\left(\sigma^2-\frac{G^2}{\omega^2}\right)=0 \quad (19)$$

which has the solution

$$\lambda=-\left(2\mu+\frac{f_2}{\omega}\cos(\alpha)\right)\pm\sqrt{\left(\sigma^2-\frac{G^2}{\omega^2}\right)} \quad (18)$$

In a similar manner, one can obtain the following eigenvalues for the stability of the trivial subharmonic resonant solution with negative CVF control

$$\lambda=-\left(2\mu+\frac{f_2}{\omega}\cos(\alpha)\right)\pm\sqrt{\sigma^2} \quad (19)$$

Consequently, the linear solution is stable for all negative values of the real part of the obtained eigenvalues.

4.4. Analytical Results

In this section, the fixed point response of the system is obtained by solving the frequency response equations (14) and (15) numerically. The representative solutions are illustrated by the amplitude-detuning parameter plots of Figs. (8), (9) and by the amplitude-force plots of Figs. (10), (11) with LPF and CVF controls for different values of other parameters.

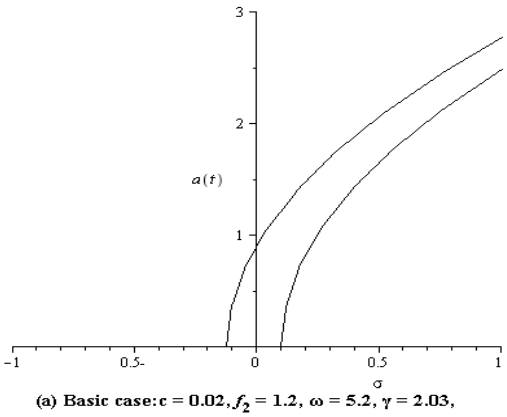

(a) Basic case: c = 0.02, f_2 = 1.2, ω = 5.2, γ = 2.03, G = 0.1, α = 10.0 deg.

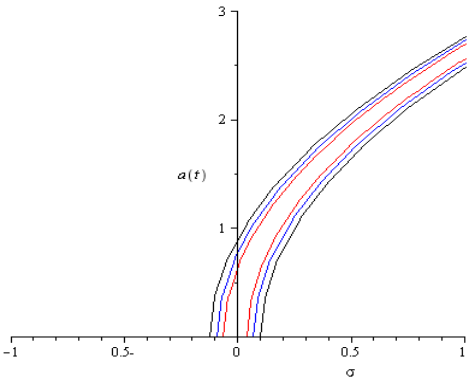

(b) Effect of varying damping coeff: μ = 0.08 (blue), 0.1 (red)

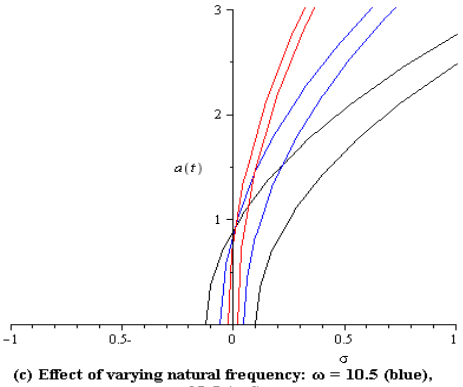

(c) Effect of varying natural frequency: ω = 10.5 (blue), 20.5 (red)

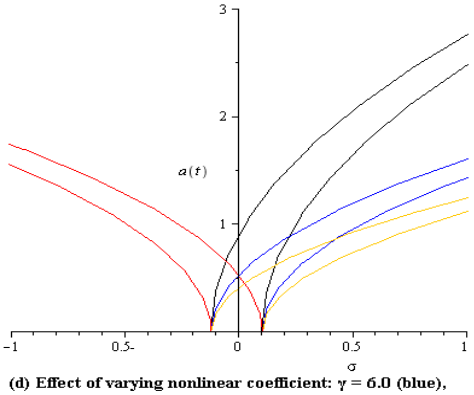

(d) Effect of varying nonlinear coefficient: γ = 6.0 (blue), 10.0(orange), -5.0 (red)

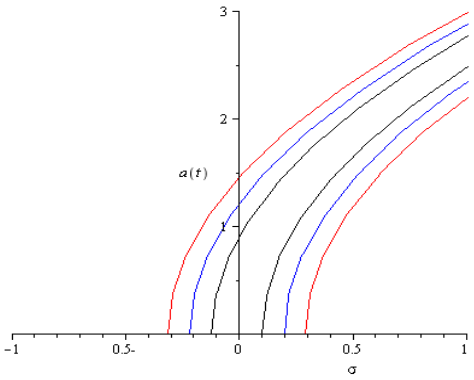

(e) Effect of varying parametric forcing amplitude: f_2 = 2.0 (blue), 3.0(red)

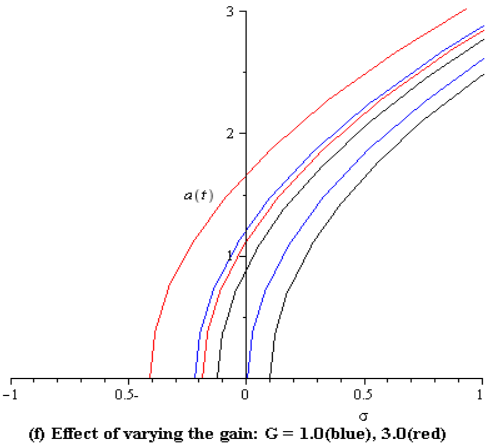

(f) Effect of varying the gain: G = 1.0(blue), 3.0(red)

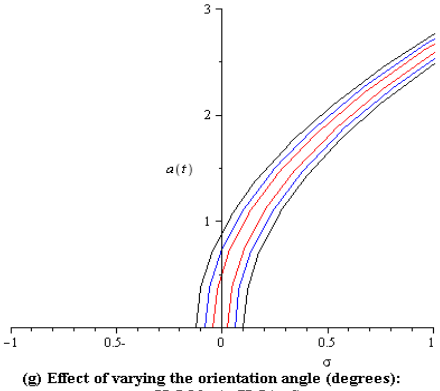

(g) Effect of varying the orientation angle (degrees): α = 50.0(blue), 70.0(red)

Figure 8. Principal parametric frequency response curves with LPF controller

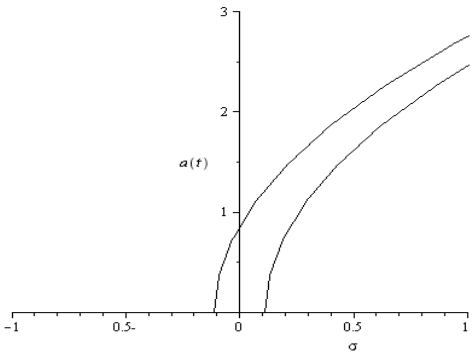

(a) Bsic casec = 0.02, f_2 = 1.2, ω = 5.2, γ = 2.03, G = 0.0001, α = 10.0 *deg*.

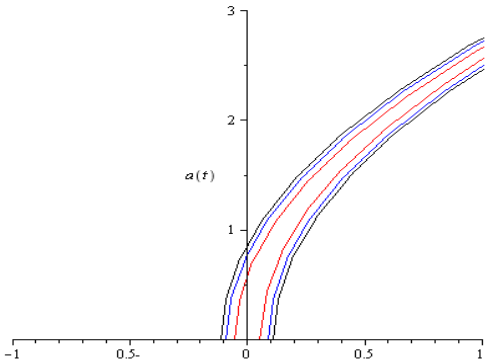

(b) Effect of varying the damping: μ = 0.07(blue), 0.1(red)

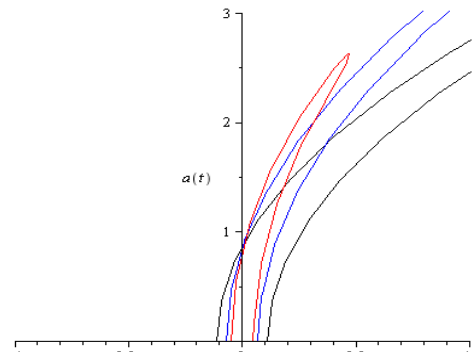

(c) Effect of varying the natural frequency: ω = 8.0(blue), 11.0(red)

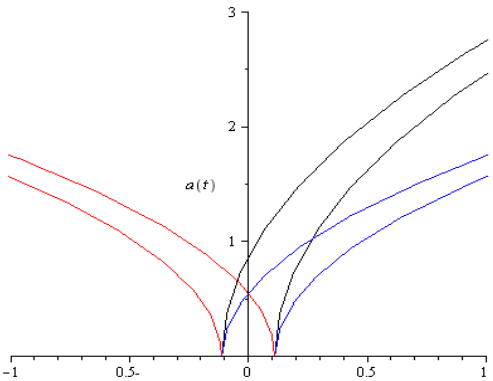

(d) Effect of varying the nonlinear term: γ = 5.0(blue), -5.0(red)

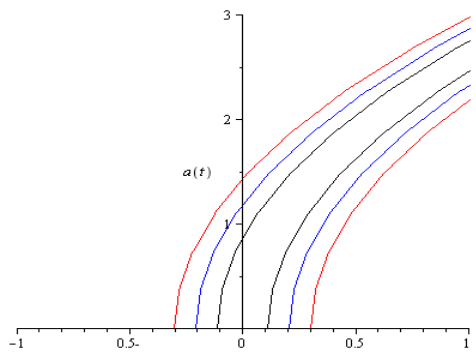

(e) Effect of varying the parametric force: f_2 = 2.0(blue), 3.0(red)

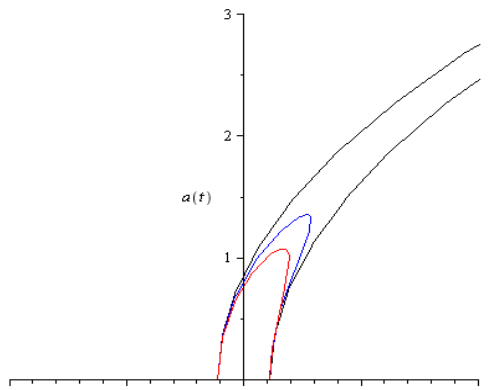

(f) Effect of varying the gain: G = 0.005(blue), 0.008(red)

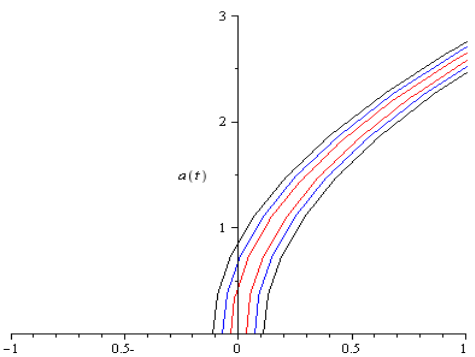

(g) Effect of varying the orientation angle (degrees): α = 50.0(blue), 70.0(red)

Figure 9. Principal parametric frequency response curves with CVF controller

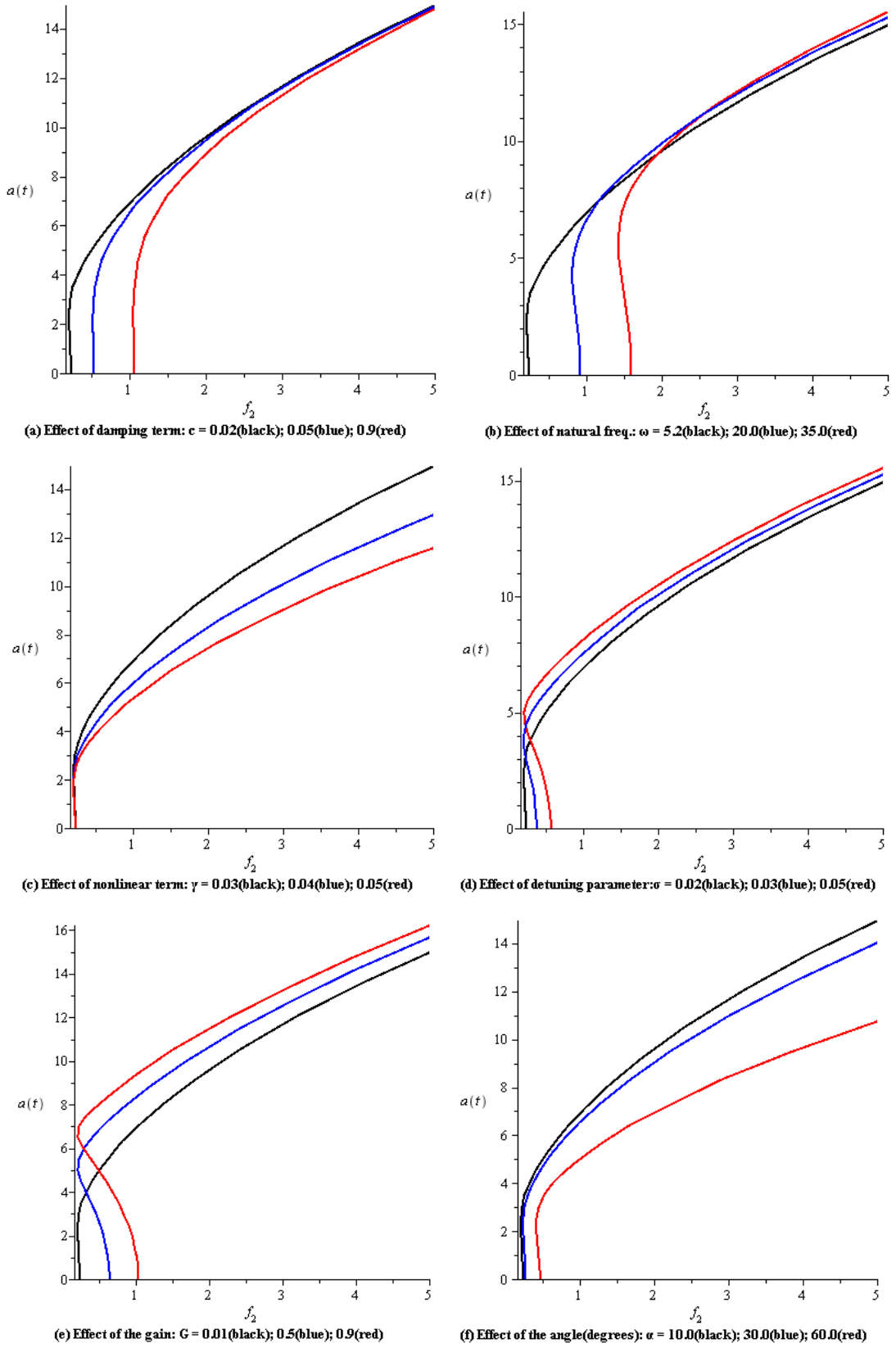

Figure 10. Principal parametric force response curves with LPF controller

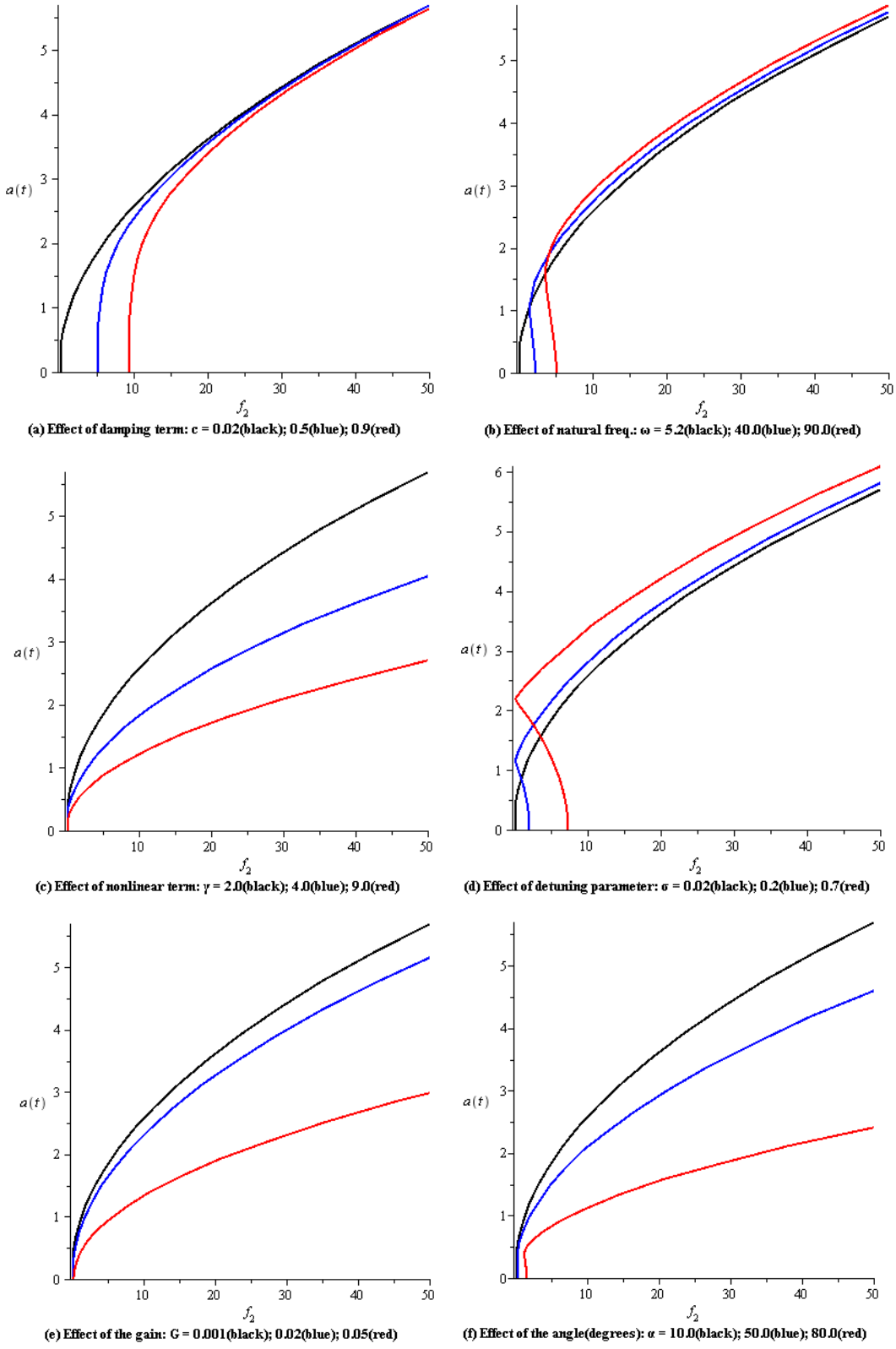

Figure 11. Principal parametric force response curves with CVF controller

4.4.1. Frequency-Response Curves

Table 2 summarizes the effect of system parameters on the frequency response curves and on the steady-state amplitude.

Comparing the effects of the system parameters in the numerical solution results, table 1, and in the frequency-response results, table 2, indicates that both results are in a good agreement.

Table 2. Results of the frequency-response curves

Parameters	LPF controller		CVF controller	
Damping coefficient μ	M.D.	Fig. 8b	M.D.	Fig. 9b
Natural frequency ω	M.I.*	Fig. 8c	M.I.*	Fig. 9c
Cubic nonlinear term γ	M.D+ H&S	Fig. 8d	M.D+ H&S	Fig. 9d
Parametric force amplitude f_2	M.I.	Fig. 8e	M.I.	Fig. 9e
The Gain G	Shift	Fig. 8f	M.D.	Fig. 9f
Orientation angle α	M.D.	Fig. 8g	M.D.	Fig. 9g

where M.I and M.D. denote the same meaning mentioned in table 1.
H&S means that the parameter has hardening and softening nonlinearity effect.
* Also the instability interval of the trivial solution decreases as ω increases and the curves are shifted to left.

4.4.2. Force-Response Curves

Figures (10) and (11) show the amplitude a as a function of the parametric forcing amplitude f_2 with LPF and CVF controls, respectively, as system parameters are varied. It can be seen that magnitude of the steady-state amplitude of the beam is monotonically increasing function in f_2.

(a) Effect of the damping coefficient μ

Figures 10(a) and 11(a) indicate that the continuous curves are shifted to the right as μ is increased with decreasing amplitude. The amplitude saturates when $f_2 > 1.0$ and $f_2 > 10.0$ for the force-response curves with LPF and CVF controllers, respectively.

(b) Effect the natural frequency ω

The force-response curves in Figs. 10(b) and 11(b) are being shifted to the right as ω increases and the amplitude increases.

(c) Effect the cubic nonlinear coefficient γ

From Figs. 10(c) and 11(c), the steady-state amplitude decreases as γ increases.

(d) Effect the detuning parameter σ

It is noticed that when σ is increased, the continuous curves shift to the right with increasing amplitude and the region of multivaludeness is defined in large intervals, as shown in Figs. 10(d) and 11(d).

(e) Effect the gain G

Figure 10(e) indicates that the effect of G on the resonant force-response curves with LPF control is similar to the effect of the detuning parameter σ. But the curves with CVF, Fig. 11(e), are shifted downward and the steady-state amplitude decreases significantly as G increases.

(f) Effect the orientation angle α

It can be seen from Figs. 10(f) and 11(f) that the steady-state amplitude gets smaller as α increases. Further increase in α lead the continuous curves to be shifted to the right with significant decrease in the amplitude.

5. Conclusions

The principal parametric vibrations of a varying orientation cantilever beam are investigated and different controllers are proposed to control the periodic and chaotic responses of the first mode of the beam when subjected to external and parametric excitations. The numerical solution is obtained at non-resonant case and principal parametric resonance case under different initial conditions and various control laws. It is found that the nonlinear cantilever beam is sensitive to initial conditions, and the best performance among positive position feedback controllers can be achieved by the LPF one. Whereas the CVF control may perform the best among velocity feedback controllers. The eigenvalues of the corresponding Jacobian matrix are determined to study the stability of the system and the analytic frequency- response curves at resonance. The effect of different parameters is investigated analytically and is verified by numerical simulations. From the study, the following may be concluded.

The multivalued solutions appear and the jump phenomenon exists in the subharmonic frequency-response curves with LPF and CVF controllers for all the system parameters. Moreover, the steady-state amplitude is a monotonic decreasing function in the damping coefficient μ, the cubic nonlinear term γ and the orientation angle α. When the natural frequency ω increases, the instability region decreases and the curves are bent to the left. The gain G in the LPF and CVF controls show different effects in the resonant frequency curves, where the continuous frequency curves shift to the left as G in the LPF control increases. But these curves indicate that the steady-state amplitude decreases as G in the CVF is increased. The nonlinearity effect (hardening or softening-type) appears for positive and negative values of the cubic nonlinear parameter γ.

From the subharmonic force-response curves with LPF and CVF controllers, it is observed that the steady-state amplitude is a monotonic increasing function in the parametric forcing amplitude f_2. The continuous curve of the steady-state amplitude shifts to the right and has (decreasing) or (increasing) stable magnitudes when the values of the parameters (μ, α) or (ω, σ, G of LPF) increase, respectively. The force-response curves shift downwards and the amplitude decreases when the cubic nonlinear parameter γ and the gain G of CVF increase.

REFERENCES

[1] Avramov, K.V, A qualitative analysis of the subharmonic oscillations of a parametrically excited flexible rod. Inter J Non-linear Mech, 39. 741–752. 2006.

[2] Yaman, M. and Sen, S, Vibration control of a cantilever beam of varying orientation. Inter J Solids Struct, 44. 1210–1220. 2007.

[3] Hegazy, U.H, Single-mode response and control of a hinged-hinged flexible beam. Arch Appl Mech, 79. 335–345. 2009.

[4] El-Bassiouny, A. F, Single-mode control and chaos of cantilever beam under primary and principal parametric excitations. Chaos, Solitons Fractals, 30(5). 1098–1121. 2005.

[5] Zhang W., Chaotic motion and its control for nonlinear nonplanar oscillations of a parametrically excited cantilever beam, Chaos, Solitons Fractals, 26. 731–745. 2005.

[6] Zhang, W., Wang, F. and Yao, M, Global bifurcation and chaotic dynamics in nonlinear nonplanar oscillations of a parametrically excited cantilever beam. Nonlinear Dyn, 40. 251–279. 2005.

[7] Nayfeh, A.H, Interaction of fundamental parametric resonances with subharmonic resonances of order one-half. J Sound Vib., 96(3). 333–340. 1984

[8] Emam, S.A. and Nayfeh, A.H, Nonlinear response of buckled beams to subharmonic-resonances excitations. Nonlinear Dyn. 35, 105-122. 2004.

[9] El-Bassiouny, A. F, Nonlinear vibration of apost-buckled beam subjected to external and parametric excitations. Physica Scripta, 74. 39–54. 2006.

[10] Hegazy, U.H, Dynamics and control of a self-sustained electromechanical seismograph with time-varying stiffness. Mecanica, 44, 355-368. 2009.

[11] Yaman, M, Direct and parametric excitation of a nonlinear cantilever beam of varying orientation with time-delay feedback. J. Sound Vib., 324, 892-902. 2009.

[12] Siewe Siewe, M. and Hegazy, U.H, Homoclinic bifurcation and chaos control in MEMS resonators, 35, 5533-5552. 2011.

[13] Younesian, D., Hargarnovin, M.H., Thompson, D.J. and Jones, C.J.C, Parametrically excited vibration of a Timoshenko beam on randon viscoelastic foundation subjected to a harmonic moving load. 45(1), 75-93. 2006.

[14] Ghayesh, M.H, Subharmonic dynamics of an axially accelerating beam. Arch Appl Mech. 82(9). 1169-1181. 2012.

[15] Mahmodi, S.N., Jalili, N. and Ahmadian, M, Suharmonic analysis of nonlinear flexural vibration of piezoelectrically actuated microcantilevers. Nonlinear Dyn. 59, 397-409. 2010.

[16] Malas, A. and Chatterjee, S, Modal self-excitation by nonlinear acceleration feedback in a class of mechanical systems. J. Sound Vib., 376, 1-17. 2016.

[17] Malas, A. and Chatterjee, S, Analysis and synthesis of modal and non-modal self-excied oscillations in a class of mechanical systems with nonlinear velocity feedback. J. Sound Vib., 334, 296-318. 2015.

[18] Pi, Y. and Ouyang, P, Vibration control of beams subjected to a moving mass using successively combined control method. Appl. Math. Modell., 40(5-6), 4002-4015. 2016.

[19] Omidi, E. and Mahmoodi, S, Sensitivity analysis of the nonlinear integral positive position feedback and integral resonant controllers on vibration suppression of nonlinear oscillatory systems. Commu. Nonlinear Sci. Numer. Simul. 22(1-3), 149-166. 2015.

[20] Eissa, M., Kandil, A., Kamel, M. and El-Ganaini, W. A, On controlling the response of primary and parametric resonances of a nonlinear magnetic levitation system. Meccanica. 50(1), 233-251, 2015.

[21] Pourseifi, M., Rahmani, O. and Hoseini, S.A.H, Active vibration control of nanotube structures under a moving nanoparticle based on the nonlocal continuum theories. Meccanica. 50(5), 1351-1369. 2015.

[22] Balthazar, J.M., Bassinello, D.G, Tusset, A.M, Bueno, A.M. and Pontes Junior, B.R, Nonlinear control in an electromechanical transducer with chaotic behavior. Meccanica. 49(8), 1859-1867. 2014.